



A Satellite-Based Model for Estimating Latent Heat Flux From Urban Vegetation

Ian A. Smith^{1*}, Joy B. Winbourne^{1,2}, Koen F. Tieskens³, Taylor S. Jones¹, Fern L. Bromley¹, Dan Li¹ and Lucy R. Hutya¹

¹ Department of Earth and Environment, Boston University, Boston, MA, United States, ² Department of Earth, Environmental, and Atmospheric Sciences, University of Massachusetts Lowell, Lowell, MA, United States, ³ Department of Environmental Health, Boston University, Boston, MA, United States

OPEN ACCESS

Edited by:

Galina Churkina,
Potsdam Institute for Climate Impact
Research (PIK), Germany

Reviewed by:

Cristina Milesi,
National Aeronautics and Space
Administration (NASA), United States
Iryna Dronova,
University of California, Berkeley,
United States

*Correspondence:

Ian A. Smith
iasmith@bu.edu

Specialty section:

This article was submitted to
Urban Ecology,
a section of the journal
Frontiers in Ecology and Evolution

Received: 15 April 2021

Accepted: 09 August 2021

Published: 30 August 2021

Citation:

Smith IA, Winbourne JB,
Tieskens KF, Jones TS, Bromley FL,
Li D and Hutya LR (2021) A
Satellite-Based Model for Estimating
Latent Heat Flux From Urban
Vegetation.
Front. Ecol. Evol. 9:695995.
doi: 10.3389/fevo.2021.695995

The impacts of extreme heat events are amplified in cities due to unique urban thermal properties. Urban greenspace mitigates high temperatures through evapotranspiration and shading; however, quantification of vegetative cooling potential in cities is often limited to simple remote sensing greenness indices or sparse, in situ measurements. Here, we develop a spatially explicit, high-resolution model of urban latent heat flux from vegetation. The model iterates through three core equations that consider urban climatological and physiological characteristics, producing estimates of latent heat flux at 30-m spatial resolution and hourly temporal resolution. We find strong agreement between field observations and model estimates of latent heat flux across a range of ecosystem types, including cities. This model introduces a valuable tool to quantify the spatial heterogeneity of vegetation cooling benefits across the complex landscape of cities at an adequate resolution to inform policies addressing the effects of extreme heat events.

Keywords: latent heat flux, evapotranspiration, urban heat island, greenspace, vegetation model

INTRODUCTION

Urban areas make up only a small fraction of global land area (<3%; Liu et al., 2014), but have a disproportionately large influence on human quality of life and well-being. Cities are home to the majority of the world's population (Grimm et al., 2008) and continue to grow in both spatial extent (Seto et al., 2012) and population (United Nations Department of Economic and Social Affairs Population Division, 2018). Urbanization often leads to environmental degradation, prompting cities to implement policies to ameliorate the environmental impacts. Such policies, however, are currently limited by a dearth of actionable urban ecological data and theory to implement demonstrated best practices (Zhou et al., 2019).

Urbanization disrupts the background surface energy balance via higher amounts of impervious surface area (ISA), increased thermal admittance of surface materials, lower albedo due to the presence of buildings and urban canyons, and fluxes of anthropogenic heat from buildings and automobiles (Oke et al., 2017). In many regions, the modified thermal characteristics of the urban landscape result in excessive heat, thermal discomfort of residents, and an urban heat island (UHI) effect, where temperatures within the city tend to exceed those of local rural environments (Taha, 1997). Historically, the primary driver of extreme urban daytime temperatures has been thought

to result from decreases in daytime latent heat flux (λE) due to higher fractions of ISA, less vegetation, less moisture availability, and therefore less evapotranspiration (Carlson and Boland, 1978; Taha, 1997). Novel attribution methods evaluating the component contributions of net radiation, aerodynamic resistance, the Bowen ratio (or ratio of sensible heat flux to λE), and heat storage provide evidence supporting the theory that the daytime UHI intensity is mostly controlled by variations in the capacity of urban and rural environments to evaporate water (Li et al., 2019). The UHI is often cited as grounds for improving urban heat resilience but is not necessarily a phenomenon that requires mitigation due to the dependence of UHI magnitude on the background rural conditions (Martilli et al., 2020). For example, some cities that do not experience a large daytime UHI (e.g., Phoenix, AZ, United States; Chow et al., 2012) still experience extreme summer temperatures. Instead, urban heat mitigation should focus on absolute temperature reduction. Nonetheless, the role of evapotranspiration in moderating extreme heat in cities points to municipal greening initiatives as promising pathways for urban heat mitigation.

Cities are warming at a faster rate than their rural counterparts (Fitzpatrick and Dunn, 2019) with increases in the magnitude and frequency of extreme weather events. Excessively high temperatures can increase electricity demand (McPherson et al., 1994; Ruijven et al., 2019), induce vegetation stress (Wahid et al., 2007; Reinmann and Hutyrá, 2017), and represent a critical risk factor for human mortality (Basu, 2009; Gasparrini et al., 2015). Many city governments have undertaken efforts to increase canopy cover (Roman, 2014) to offset local climate changes driven by urbanization. Common surface materials found in the urban environment are impervious and do not retain much moisture for evaporation. Vegetation, however, can be used as a tool to cool the urban environment via evapotranspiration. When plants open their stomata to take up carbon dioxide (CO_2), they simultaneously release water vapor in a process that utilizes energy for the conversion of liquid water to a vapor state, cooling the plant and the air around it. Remote sensing observations reveal an inverse relationship between surface temperature and the Normalized Difference Vegetation Index (Tiangco et al., 2008) and field experiments have shown that rooftop gardens can reduce the surface temperature of buildings and the air around them (Wong et al., 2003). Ziter et al. (2019) found the proportions of canopy cover and ISA to be interactive drivers of urban temperature variation. While previous research has established the potential for vegetative cooling in urban environments, less attention has been given to quantifying evapotranspiration rates and the corresponding λE variations across entire cities.

Direct measurements of λE at discrete locations are commonly made using eddy covariance flux towers. However, this technique assumes uniform vegetation canopies on flat terrain (Munger and Loeschner, 2004). The heterogeneous landscape associated with cities often violates some assumptions embedded in eddy covariance methodologies, making urban measurements difficult. Consequently, direct measurements of λE in urban areas are often made using tree-level measurements of evapotranspiration. While this can be done by taking leaf-level measurements of transpiration rates that are then scaled to the

entire canopy, studies more commonly use measurements of sap flux rates in trees (Pataki et al., 2011; Winbourne et al., 2020). Sap flux measurements provide an integrative measure of water use and transpiration yielding important information about the energy balance of individual trees. Modeling approaches are necessary, however, to capture the spatial variability in λE across larger areas of interest.

The Penman-Monteith model (Monteith, 1965) is a commonly used approach to estimate λE based primarily on meteorological conditions and the capacity of the land surface to transfer water into the lower atmosphere. Recent Penman-Monteith applications have started to focus on urban areas (Liu et al., 2017; Zipper et al., 2017; Zhang et al., 2018; Wang et al., 2020), incorporating the unique climatological properties of cities by including the UHI (Zipper et al., 2017) and spectral mixture analysis to consider the unique physical structure of urban areas (Wang et al., 2020). Results show higher atmospheric demand for water in areas with higher amounts of ISA and alleviation of the UHI in regions with high evapotranspiration intensity (Zipper et al., 2017; Wang et al., 2020). Other models exist to partition surface energy fluxes in cities, however, the International Urban Energy Balance Comparison Project (Grimmond et al., 2010) found that the most commonly used models had the poorest performance in modeling the λE component of the surface energy balance and highlighted the importance of accurate representation of vegetation in correctly modeling the partitioning of turbulent fluxes. The focus on quantifying evapotranspiration in urban areas is advancing our knowledge of the surface energy balance within cities; however, urban vegetation exhibits unique physiological dynamics that to our knowledge have not yet been captured in previous studies (Winbourne et al., 2020).

Urban vegetation tends to grow at accelerated rates compared to rural vegetation (Briber et al., 2015; Smith et al., 2019), likely due to a combination of increased light availability due to open grown conditions, higher nitrogen (Rao et al., 2014; Decina et al., 2017) and phosphorus (Hobbie et al., 2017; Decina et al., 2018) deposition rates, higher surface CO_2 concentrations (Bronfield et al., 2012), lengthened growing seasons (Melaas et al., 2016) and in some cases, higher water availability (McCarthy and Pataki, 2010; Bijoer et al., 2011). Faster plant growth has important effects on stomatal conductance, the process governing the exchange of water vapor between the biosphere and the atmosphere, due to the strong coupling between the processes of photosynthesis and transpiration. Studies of the relationship between stomatal conductance and temperature in controlled experiments come to inconsistent conclusions (Weston and Bauerle, 2007; Teskey et al., 2014; von Caemmerer and Evans, 2015; Urban et al., 2017). While similar urban studies are rare, Winbourne et al. (2020) found a stronger positive relationship between stomatal conductance and temperature in urban versus rural settings with observations of persistent stomatal conductance in an urban maple tree at temperatures in excess of 30°C and vapor pressure deficits (VPD) greater than 2.5 kPa. Furthermore, Esperon-Rodriguez et al. (2020) found evidence of urban tree adaptation to climate via plasticity in drought tolerance traits, with urban trees of

the same species exhibiting more drought tolerance than rural trees. This suggests that urban trees may have the ability to acclimate to the extreme growing conditions found in the urban environment, underscoring the role of urban vegetation in providing temperature relief during extreme heat events.

Here, we introduce the Vegetation Photosynthesis and Respiration Model Latent Heat module (VPRM-LH) – a spatially explicit, remote sensing-driven model to produce hourly estimates of urban λE at 30 m spatial resolution. In contrast to frequently used vegetation indices characterizing the extent of urban greenspace, VPRM-LH explicitly includes information about the function of urban greenspace and its variation across space and time. VPRM-LH outputs are particularly relevant to the implementation of nature-based climate solutions in cities due to a specific focus on vegetation contributions to λE . We find strong agreement between field observations and model estimates of λE across a range of ecosystems and urbanization intensities, highlighting VPRM-LH as an effective tool in quantifying the spatial heterogeneity of vegetation cooling benefits within cities.

METHODS

As an overview, VPRM-LH iterates through three core equations that consider urban structural, climatological, and physiological characteristics. Surface conductance of water vapor is estimated as a function of photosynthesis and VPD using the Urban Vegetation Photosynthesis and Respiration Model (VPRM) (Mahadevan et al., 2008; Hardiman et al., 2017) and Medlyn stomatal conductance model (Medlyn et al., 2011). The Penman-Monteith model is used to produce estimates of λE , with meteorological inputs downscaled to 30 m resolution based on empirical relationships between ISA and temperature/VPD (Wang et al., 2017). We present the necessary model equations and data specifications to apply the VPRM-LH framework (summarized in **Supplementary Table 1**). Model equations were executed in R version 3.6 (R Core Team, 2020).

Model Description

Vegetation Photosynthesis and Respiration Model

We use the VPRM hourly carbon exchange as a means to estimate net photosynthesis and eventually stomatal conductance. Photosynthesis is defined as the gross biosphere-atmosphere ecosystem exchange (GEE; $\mu\text{mol CO}_2 \text{ m}^{-2} \text{ s}^{-1}$) of CO_2 and is estimated as a function of incoming photosynthetically active radiation (PAR) using a modified version of the Urban VPRM, introduced in Hardiman et al. (2017). The first of three core equations in VPRM-LH is:

$$GEE = \Lambda \cdot T_{scale} \cdot P_{scale} \cdot W_{scale} \cdot EVI \cdot \frac{1}{1 + \frac{PAR}{PAR_0}} \cdot PAR \quad (1)$$

where T_{scale} , P_{scale} , and W_{scale} are dimensionless scaling terms ranging from zero to one describing the influence of air temperature, phenology, and moisture on photosynthesis. Λ and PAR_0 are ecosystem-specific parameters describing the light-use efficiency of vegetation and half-saturation value of GEE as a function of PAR. EVI is the enhanced vegetation index.

For rural applications, T_{scale} is calculated following the equations within the original VPRM parameterization (Mahadevan et al., 2008) as:

$$T_{scale} = \frac{(T - T_{min})(T - T_{max})}{(T - T_{min})(T - T_{max}) - (T - T_{opt})^2} \quad (2)$$

where T is the air temperature, T_{min} is the minimum temperature for photosynthesis, T_{max} is the maximum temperature for photosynthesis, and T_{opt} is the ecosystem-specific optimal temperature for photosynthesis. For urban applications, however, the T_{scale} equation is used for temperatures less than 20°C , but is set to one for all temperatures greater than 20°C to account for acclimation of urban vegetation to warmer temperatures. Our field observations of sap flux indicate that stomatal activity does not shut down in urban trees at temperatures up to 35.5°C , the highest observed temperature in the measurement period (**Supplementary Figure 1**). In this model, we set the maximum temperature for photosynthesis in both urban and rural pixels to 40°C . P_{scale} captures the impact of leaf age on vegetation activity and is calculated as:

$$P_{scale} = \frac{EVI - EVI_{min}}{EVI_{max} - EVI_{min}} \quad (3)$$

where EVI_{min} and EVI_{max} are the minimum and maximum EVI observed during the growing season.

W_{scale} is a function of the Land Surface Water Index (LSWI), which has been shown to be effective in monitoring vegetation water content (Maki et al., 2004; Gu et al., 2008), and is calculated as:

$$W_{scale} = \frac{1 + LSWI}{1 + LSWI_{max}} \quad (4)$$

where $LSWI_{max}$ is the maximum LSWI observed during the growing season.

Ecosystem respiration, required to estimate net photosynthesis (A_n ; $\mu\text{mol CO}_2 \text{ m}^{-2} \text{ s}^{-1}$) at the leaf level, is calculated as:

$$R_{eco} = T \cdot \alpha + \beta \quad (5)$$

where T is the air temperature ($^\circ\text{C}$), α is the sensitivity of R_{eco} to T , and β is the minimum value that R_{eco} can take on ($\mu\text{mol CO}_2 \text{ m}^{-2} \text{ s}^{-1}$). Leaf respiration typically accounts for 8–12% of ecosystem respiration (Tang et al., 2008) and is approximated to be 10% of R_{eco} . Therefore, net photosynthesis of the canopy is estimated as:

$$A_n = GEE - 0.1 \cdot R_{eco} \quad (6)$$

VPRM driver data come from publicly available remote sensing and modeling products. EVI and LSWI are calculated at 30 m resolution using Landsat 7 and Landsat 8 Tier 1 Surface Reflectance products retrieved from Google Earth Engine (Gorelick et al., 2017; Dwyer et al., 2018). Using data from two Landsat sensors allows for EVI to be obtained every 8 days. Daily EVI values are interpolated between collection dates using a spline function (**Supplementary Figure 2**). PAR data come from

the Geostationary Operational Environmental Satellite (GOES; EUMETSAT OSI SAF, 2021b) 16 which provides high spatial ($0.05^\circ \times 0.05^\circ$) and temporal (hourly) resolution datasets of incoming shortwave radiation (SW; $W m^{-2}$) to North America. In our study, PAR ($\mu mol m^{-2} s^{-1}$) is approximated to be $SW/0.505$ (Mahadevan et al., 2008). Hourly temperature data come from the Rapid Refresh analysis product (RAP; Benjamin et al., 2016) at a native resolution of $13 km \times 13 km$. Temperature data are adjusted as a linear function of ISA (MassGIS, 2019) and hour of year using the coefficients derived in Wang et al. (2017) and methods described in Hardiman et al. (2017).

Medlyn Stomatal Conductance Model

Given estimates of photosynthesis, surface conductance at 30 m resolution is estimated using the Medlyn et al. (2011) as:

$$g_s = g_0 + 1.6 \cdot \left(1 + \frac{g_1}{\delta}\right) \cdot \frac{A_n}{\frac{c_s}{P_{atm}}} \quad (7)$$

where g_s is the surface conductance ($\mu mol H_2O m^{-2} s^{-1}$), g_0 is the minimum surface conductance ($100 \mu mol H_2O m^{-2} s^{-1}$), g_1 is a unitless plant functional type dependent parameter that captures the sensitivity of surface conductance to photosynthesis rate (de Kauwe et al., 2015), δ is the VPD (kPa), A_n is net photosynthesis ($\mu mol CO_2 m^{-2} s^{-1}$), c_s is the partial pressure of CO_2 (40.53 Pa), and P_{atm} is the atmospheric pressure (101325 Pa). P_{atm} and c_s are held constant due to little sensitivity of model outputs to variations in the values. δ is calculated from RAP temperature and relative humidity, where values are adjusted to account for urban heat and dry islands as a linear function of ISA and hour of year using the coefficients derived in Wang et al. (2017).

Penman-Monteith Model

Given estimates of surface conductance, λE ($W m^{-2}$) is calculated using the Penman-Monteith model as:

$$\lambda E = \frac{\Delta(R_n - G) + \rho_a c_p (\delta) g_a}{\Delta + \gamma \left(1 + \frac{g_a}{g_s}\right)} \quad (8)$$

where λ is the latent heat of vaporization of H_2O ($2260 J g^{-1}$), E is the mass H_2O evaporation rate ($g s^{-1} m^{-2}$), Δ describes the rate of change of saturation specific humidity with air temperature ($Pa K^{-1}$), R_n is the net radiation balance of the surface ($W m^{-2}$), G is the ground heat flux ($W m^{-2}$), ρ_a is the dry air density ($1.275 kg m^{-3}$), c_p is the specific heat capacity of air ($1005 J kg^{-1} K^{-1}$), δ is the VPD (Pa), g_a is the atmospheric conductance ($m s^{-1}$), g_s is the surface conductance ($m s^{-1}$), and γ is the psychrometric constant ($66 Pa K^{-1}$).

Δ is calculated following the methods outlined in Allen et al. (1998) as:

$$\Delta = \frac{4098[0.6108 \exp(\frac{17.27T}{T+237.3})]}{(T + 237.3)^2} \quad (9)$$

where T is the ISA-adjusted air temperature. R_n is calculated as:

$$R_n = (1 - \alpha) K \downarrow + L \downarrow - (\epsilon \sigma T_s^4 + (1 - \epsilon) L \downarrow) \quad (10)$$

where α is the albedo (Trlica et al., 2017), $K \downarrow$ is incoming shortwave radiation ($W m^{-2}$; GOES-16), $L \downarrow$ is incoming longwave radiation ($W m^{-2}$; EUMETSAT OSI SAF, 2021a), ϵ is the surface emissivity (Estimated to be 0.95 in urban areas; Oke et al., 2017), σ is the Stefan-Boltzmann constant ($5.67 \times 10^{-8} W m^{-2} K^{-4}$), and T_s is the surface temperature (K; RAP). G is approximated as 10% of R_n . ρ_a and c_p are held constant as the model outputs show little sensitivity to variations in their values (Supplementary Figure 3). Previous work found λE estimates to be relatively insensitive to variation in g_a within the range of 0.010 – $0.033 m s^{-1}$ (Zhang and Dawes, 1995), consistent with values measured in city canopies (Chen et al., 2011; Ballinas and Barradas, 2016). We use the constant values of 0.033 and $0.010 m s^{-1}$ for forests/cities and croplands, respectively, as applied in Zhang et al. (2008).

Model Validation

Rural Validation

Vegetation photosynthesis and respiration model latent heat was validated across a range of rural ecosystem types. Three dominant North American land covers – deciduous broadleaf forest (DBF), evergreen needleleaf forest (ENF), and croplands (CRP) – were chosen as validation sites. Eddy covariance flux tower λE measurements were compared to model estimates in a $90 m \times 90 m$ grid (10 pixels) centered on the flux tower for the most recent full year of available data (2017 for ENF, 2018 for DBF and CRP).

The Harvard Forest (AmeriFlux ID: US-Ha1) in MA, United States was the validation site for DBF and is dominated by red oak (*Quercus rubra*) and red maple (*Acer rubrum*; Munger, 2021). The Howland Forest in Maine, United States (AmeriFlux ID: US-Ho1) was the validation site for ENF and is dominated by red spruce (*Picea rubens*) and eastern hemlock (*Tsuga canadensis*; Hollinger, 2021). The Nebraska Agricultural Research and Development Center (AmeriFlux ID: US-Ne1) in NE, United States was the validation site for CRP and is an irrigated maize field (Suyker, 2021).

Urban Heatwave Modeling and Validation

λE was modeled across Boston, MA, United States during mean and heatwave conditions during the summer of 2018. Mean conditions were modeled during a 6-day period from July 10–July 15, 2018 where the mean air temperature across the modeling domain was $23.1^\circ C$, approximately equal to the mean 2018 6-day rolling average temperature during June, July, and August (JJA; $23.0^\circ C$). Heatwave conditions were modeled during a 6-day heat event from August 2–August 7, 2018 where the mean air temperature across the modeling domain was $28.7^\circ C$ (Supplementary Figure 4).

Validation of urban ecosystem models can be difficult due to limited field observations. Here, outputs were validated by modeling λE in five pixels ranging from 47 to 99% ISA containing trees outfitted with sap flux sensors between July 18 and September 26, 2019. Details on sap flux sensor methodology are described in Jones et al. (2020). Validation trees were in healthy condition and included two sugar maples (*Acer saccharum*), two Norway maples (*Acer platanoides*), and one red maple

(*Acer rubrum*). λE ($W m^{-2}$) was estimated from sap flux measurements by estimating the rate of transpiration ($g H_2O s^{-1} m^{-2}$) via multiplying sap flux density ($g H_2O cm^{-2} s^{-1}$) by the active sapwood area (the fraction of the basal area cross-section that is active xylem; cm^2) and dividing by the crown area of the tree (m^2). λE ($W m^{-2}$) was then computed as the transpiration rate multiplied by the latent heat of vaporization of H_2O ($2260 J g^{-1}$). The active sapwood area of the tree was estimated from species-specific allometric equations (Wullschlegel et al., 2001; Gebauer et al., 2008). Statistical analyses were conducted in R version 3.6 (R Core Team, 2020).

RESULTS

Rural λE

We ran VPRM-LH for a full year in three rural ecosystems and compared outputs with eddy covariance flux measurements of λE . We find strong agreement between modeled and measured λE across a range of time scales, especially during the summer months (defined as JJA; **Figure 1**). Disagreement during the dormant season is likely due to a higher proportion of λE from evaporation not related to stomatal activity (e.g., evaporation from soils), rather than direct fluxes via transpiration. Modeled and measured λE show typical seasonal patterns with high rates during the warmer growing season and low rates during the cooler dormant season (**Figures 1A–C**). Modeled versus measured λE are of the same order of magnitude at hourly and daily time scales. Mean diurnal patterns in λE , including afternoon peaks and nighttime lows, are successfully captured by VPRM-LH (**Figures 1D–F**). JJA comparisons of hourly λE show a high correlation (R^2 values 0.83, 0.75, and 0.89 for DBF, ENF, and CRP, respectively; **Figures 1G–I**). The accuracy of VPRM-LH is comparable to the accuracy of VPRM estimates of net ecosystem exchange of CO_2 (NEE) as the R^2 values associated with hourly estimates of NEE for the same ecosystem types as reported in Mahadevan et al. (2008) are 0.83, 0.65, and 0.83 for DBF, ENF, and CRP, respectively.

Urban λE

λE across Boston varied substantially, with higher λE in the more vegetated portions of the city and lower λE in the more impervious portions of the city (**Figure 2A**). λE generally increased with temperature, except for cloudy days where λE was limited by available incoming solar radiation (**Supplementary Figure 4**). During the 6-day heatwave event, λE averaged $85.6 W m^{-2}$ and was approximately 17% higher than during the 6 days representing mean summer conditions ($73.1 W m^{-2}$). Daily maximum λE ranged from $135.4 W m^{-2}$ on a cloudy day to $334.5 W m^{-2}$ during the warmest day in the study period. For reference, the maximum estimated λE during JJA at the DBF site, located approximately 100 km west of Boston, was $486.4 W m^{-2}$.

The model modifications intended to capture urban λE dynamics were evaluated by comparing model estimates of λE in a subset of five pixels in Boston, MA, United States to coincident λE estimates derived from sap flux measurements within the pixels. Hourly field and model estimates of daytime λE show

a similarly strong agreement with the rural model application ($R^2 = 0.80$) across a range of urbanization intensities and tree species (**Figure 2B**).

In general, λE was lower in pixels with higher ISA (**Figures 2B, 3A**), however, for a given EVI greenness the λE increased with ISA due to urban heat and dry island impacts on local meteorological conditions (**Figure 3A**). For example, for all pixels where $EVI = 0.70$ ($n = 912$), the average 14:00 EDT λE ranged from 219.1 to $249.7 W m^{-2}$ (**Figure 3A**). Furthermore, EVI remains relatively stable on the scale of weeks during the growing season, but λE has a diurnal cycle with peak fluxes occurring during the afternoon, is close to zero at night, and responds rapidly to changes in meteorological conditions. The temporal resolution of VPRM-LH captures this diurnal pattern and shows that enhancements of λE due to urbanization during the daytime, when exposure to high temperatures is greatest, is higher than nighttime (**Figure 3B**). The average range of λE for all pixels with an $EVI = 0.70$ was less than $1 W m^{-2}$ during the night and was greater than $30 W m^{-2}$ between 12:00 and 15:00 EDT.

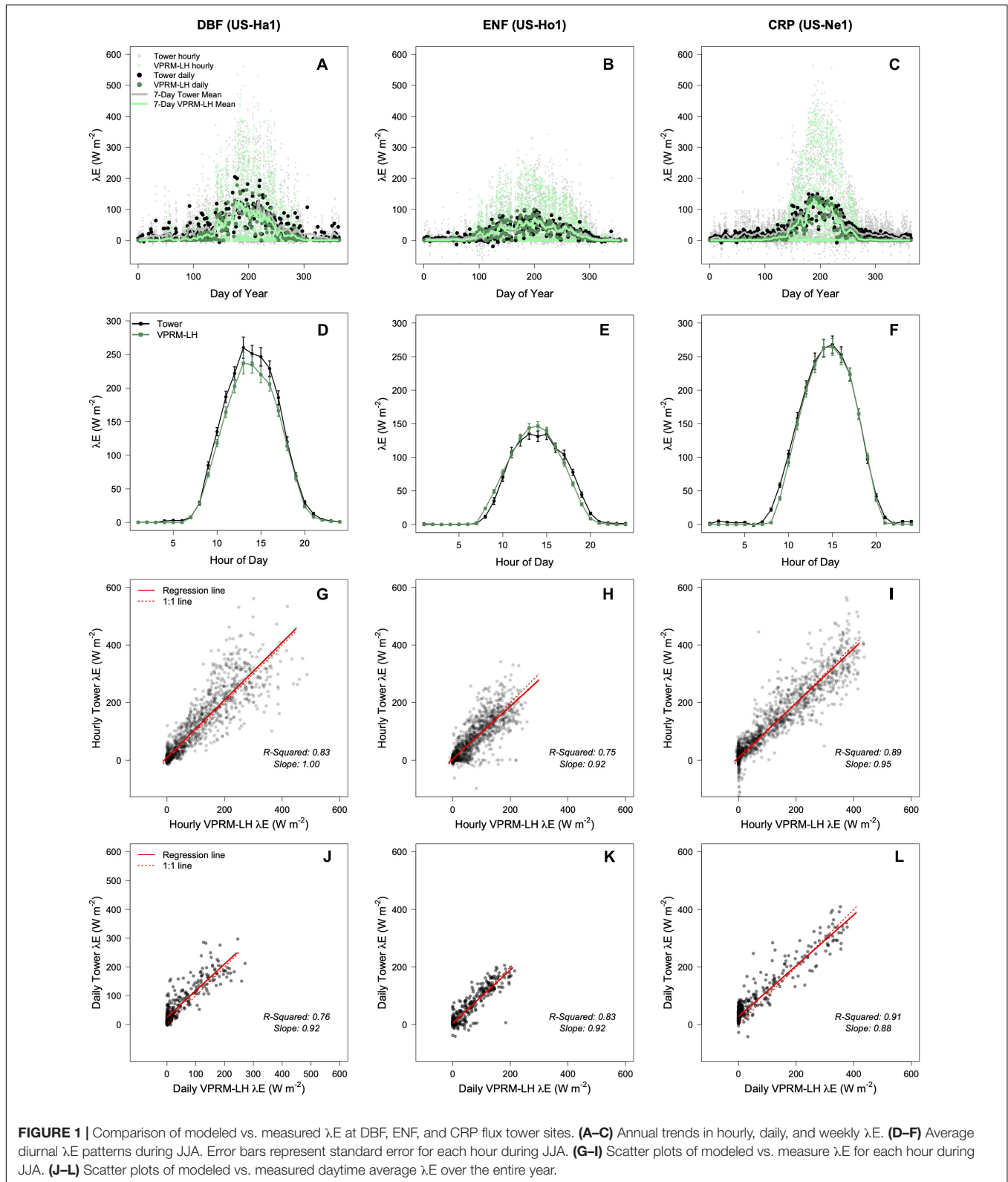
The spatial patterns of λE and EVI are similar (**Figures 2A, 3C**), however, using λE as a metric of vegetation cooling benefits captures interactive impacts of greenspace distributions, radiation, and temperature drivers (ISA; **Figure 3D**).

DISCUSSION

Cities are highly vulnerable to projected increases in mean air temperatures and the frequency of extreme heat events (Habeeb et al., 2015) and as a result are eager to obtain actionable ecological data informing their climate mitigation strategies (Zhou et al., 2019). Extreme temperatures already represent an important threat to public health, with vulnerable populations (in terms of age, race, and income) particularly susceptible to heat-related illness and death (Wellenius et al., 2017). Here, we introduce a simple tool to quantify vegetation cooling activity in cities with the potential to identify areas that will benefit most from tree planting or urban greening.

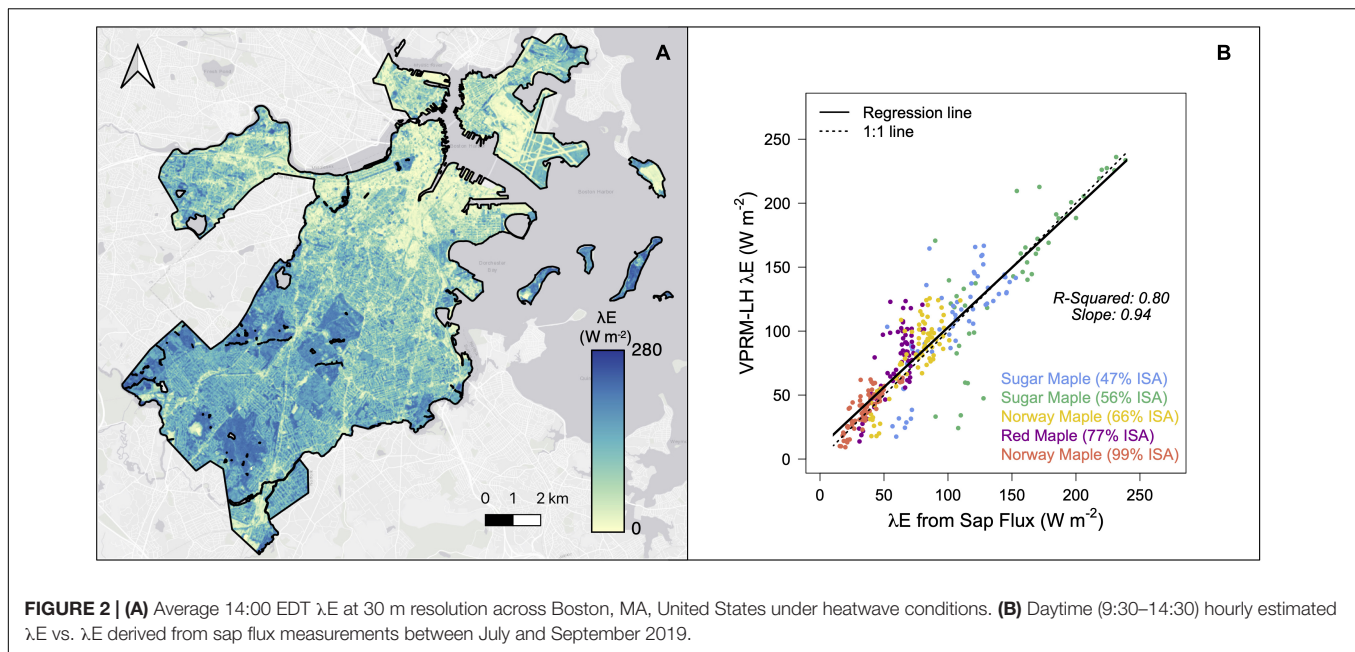
Model Implementation and Limitations

Vegetation photosynthesis and respiration model latent heat uses several readily accessible data sources such as the Landsat, GOES, and RAP archives. Urban applications require the use of an additional spatially explicit ISA product and information about the region-specific relationship between air temperature and ISA, however, this could be determined using local weather station archives or low-cost sensor networks, such as those used in Wang et al. (2017). VPRM-LH estimates λE with good accuracy across ecosystems and time scales; the model driver data is independent of the field observations used for validation. The assumptions embedded in estimation of ground heat flux, dry air density, specific heat capacity, and leaf respiration rates do not appear to introduce critical errors into λE estimates. A sensitivity analysis of the incremental change in λE resultant from incremental changes in model parameters points to the atmospheric conductance term (treated as a constant) as a main source of unaccounted for variance/uncertainty in the model



(Supplementary Figure 3). Implementation of additional data sources capturing the variability in atmospheric conductance could further improve model accuracy.

The model validation and application presented here was conducted in either mesic or irrigated ecosystems where water availability does not typically constrain transpiration. Model



application would benefit from further validation in more water-limited regions. VPRM-LH currently considers moisture limitations on transpiration in the W_{scale} term (eq. 3), which leverages LSWI to restrict vegetation activity during dry periods. The availability of water for vegetation, whether from irrigation or precipitation, is a critical consideration in determining the location for urban vegetation expansion. Additionally, VPRM-LH only distinguishes vegetation at the plant functional type level and does not consider species-specific differences in transpiration strategies (e.g., isohydric vs. anisohydric). While the omission of species-specific parameters may limit model accuracy under certain climate conditions, VPRM-LH does not require high-resolution tree species maps, which are likely not available for many cities.

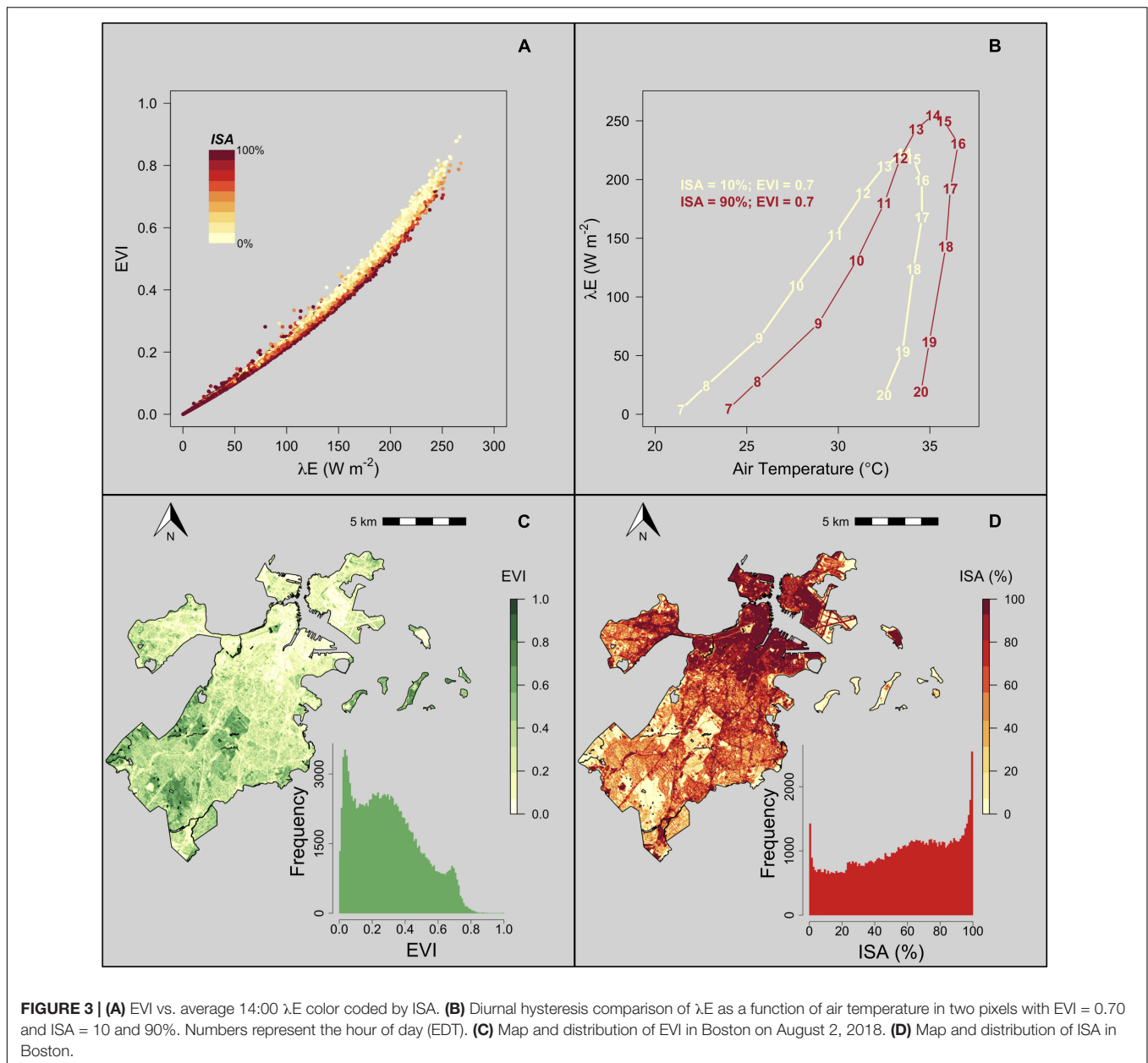
The interpretation of model outputs in mesic climates, particularly on hot, humid days, should consider more than just the magnitude of λE . Regions with a relatively high λE will have more turbulent energy fluxes partitioned into latent rather than sensible heat, which results in a cooling effect on temperature. This interpretation, however, neglects to consider the impact of the increase in atmospheric moisture (resultant from increased transpiration) on perceived temperature. Higher atmospheric humidity reduces the ability of the human body to shed excess heat via the evaporation of sweat, lowering the rate that the body can cool and increasing the perceived temperature, where the perceived temperature is commonly quantified by the heat index. In New York City, NY, United States (approximately 300 km southwest of Boston), a significant increase in mortality risk was observed on days where the maximum heat index exceeded 35° C (Metzger et al., 2010). Heat indices in excess of 35° C were not observed when modeling mean summer conditions in Boston. However, during the 6-day heatwave event, the average daily maximum temperature ranged from 27.7 to 35.7° C, with 5.7% of pixels exceeding 35° C. The average daily maximum

heat index during the same time period ranged from 29.0 to 43.9° C with 78.4% of pixels exceeding the 35° C threshold, highlighting the impact of atmospheric moisture concentration on perceived temperature.

The provision of shade, which represents another important determinant of perceived temperature, counteracts humidity effects. For example, Rahman et al. (2018) found that the daytime air temperature under urban tree canopies in a temperate climate was always lower than the air temperature in open areas. Furthermore, while λE was the predominant cooling mechanism of the air on days up to 30° C, shading effects were more prominent on extremely hot days in excess of 30° C (Rahman et al., 2018). Model output interpretation should consider the implications of atmospheric moisture inputs and the type of vegetation present, where trees will provide shade benefits that are not provided by shrubs and grasses.

Implications for Cities

Urban greening, widely espoused as a climate mitigation strategy, has been implemented around the world (Mell et al., 2013; Pincetl et al., 2013; Tan et al., 2013) despite debates around the exact services and tradeoffs with disservices provided by urban canopies. Urban vegetation does store (Raciti et al., 2014) and take up more atmospheric carbon (Sargent et al., 2018) than most ecosystem models currently account for Churkina (2008), but due to accelerated turnover (Smith et al., 2019) and respiration (Decina et al., 2016) rates, tree planting is likely not a viable avenue for meaningful carbon sequestration. Additionally, urban trees are capable of removing atmospheric pollutants and particulates (Weber et al., 2014) but are also sources of volatile organic compounds (Churkina et al., 2015) and allergens (Beck et al., 2013). The urban canopy, however, undoubtedly contributes to local cooling via shading and transpiration (Bowler et al., 2010), with temperature reductions from vegetation



observed to be up to 8°C (Rahman et al., 2017). The potential for vegetative cooling in cities is well established, but implementation of greening plans for effective urban cooling has been heretofore limited due to the inability to quantify variation in cooling potential across the complex landscape of cities.

Vegetation photosynthesis and respiration model latent heat offers a simple, satellite-based methodology for estimating urban λE contributions from vegetation at fine spatial and temporal resolution. The model incorporates a novel combination of urban-specific parameters capturing climatological, physical, and physiological intricacies of the urban environment and its components. Model outputs are consistent with ground measurements of λE and can be scaled to explore the cooling potential of vegetation across cities at hourly, diurnal, seasonal,

and annual scales. In contrast to vegetation indices that are commonly used to quantify the benefits of urban greenspace, λE captures vegetation activity in addition to abundance and offers nuanced information about the ecosystem services provided by urban vegetation. VPRM-LH will be a valuable tool in the implementation of policies combatting heat related consequences of urbanization, especially as cities take the forefront in addressing climate-related matters. VPRM-LH offers an easy implementation and the ability to combine outputs with sociodemographic datasets at sufficient resolution for political action. The result is a unique opportunity to identify vulnerable neighborhoods and optimize municipal decisions that repartition the surface energy balance to address historic inequities in canopy distribution and UHI (Hoffman et al., 2020).

DATA AVAILABILITY STATEMENT

The datasets presented in this study can be found in online repositories. The names of the repository/repositories and accession number(s) can be found below: Smith (2021). “Data for ‘A satellite-based model for estimating latent heat flux from urban vegetation,’” <https://doi.org/10.7910/DVN/TQLSIU>, Harvard Dataverse.

AUTHOR CONTRIBUTIONS

IAS, DL, and LRH conceptualized the research, developed the framework, and analyzed the data. JBW, TSJ, and FLB collected the validation data. IAS, JBW, KFT, TSJ, FLB, DL, and LRH wrote the original draft, and reviewed and edited the

REFERENCES

- Allen, R., Pereira, L., and Smith, M. (1998). *Crop Evapotranspiration. Guidelines for Computing Crop Water Requirements*. In *FAO Irrigation and Drainage Paper*, Vol. 56. Rome: FAO.
- Ballinas, M., and Barradas, V. L. (2016). The Urban tree as a tool to mitigate the urban heat island in Mexico City: a simple phenomenological model. *J. Environ. Qual.* 45, 157–166. doi: 10.2134/jeq2015.01.0056
- Basu, R. (2009). High ambient temperature and mortality: a review of epidemiologic studies from 2001 to 2008. *Environ. Health* 8:40. doi: 10.1186/1476-069x-8-40
- Beck, I., Jochner, S., Gilles, S., McIntyre, M., Buters, J. T. M., Schmidt-Weber, C., et al. (2013). High environmental ozone levels lead to enhanced allergenicity of birch pollen. *PLoS One* 8:e80147. doi: 10.1371/journal.pone.0080147
- Benjamin, S. G., Weygandt, S. S., Brown, J. M., Hu, M., Alexander, C. R., Smirnova, T. G., et al. (2016). A North American hourly assimilation and model forecast cycle: the rapid refresh. *Mon. Weather Rev.* 144, 1669–1694. doi: 10.1175/mwr-d-15-0242.1
- Bijoor, N. S., Mccarthy, H. R., Zhang, D., and Pataki, D. E. (2011). Water sources of urban trees in the Los Angeles metropolitan area. *Urban Ecosyst.* 15, 195–214. doi: 10.1007/s11252-011-0196-1
- Bowler, D. E., Buyung-Ali, L., Knight, T. M., and Pullin, A. S. (2010). Urban greening to cool towns and cities: a systematic review of the empirical evidence. *Landsc. Urban Plan.* 97, 147–155. doi: 10.1016/j.landurbplan.2010.05.006
- Briber, B. M., Hutyrá, L. R., Reinmann, A. B., Raciti, S. M., Dearborn, V. K., Holden, C. E., et al. (2015). Tree productivity enhanced with conversion from forest to urban land covers. *PLoS One* 10:e0136237. doi: 10.1371/journal.pone.0136237
- Brondfield, M. N., Hutyrá, L. R., Gately, C. K., Raciti, S. M., and Peterson, S. A. (2012). Modeling and validation of on-road CO₂ emissions inventories at the urban regional scale. *Environ. Pollut.* 170, 113–123. doi: 10.1016/j.envpol.2012.06.003
- Carlson, T. N., and Boland, F. E. (1978). Analysis of urban-rural canopy using a surface heat flux/temperature model. *J. Appl. Meteorol.* 17, 998–1013. doi: 10.1175/1520-0450(1978)017<0998:aourcu>2.0.co;2
- Chen, L., Zhang, Z., Li, Z., Tang, J., Caldwell, P., and Zhang, W. (2011). Biophysical control of whole tree transpiration under an urban environment in Northern China. *J. Hydrol.* 402, 388–400. doi: 10.1016/j.jhydrol.2011.03.034
- Chow, W. T., Brennan, D., and Brazel, A. J. (2012). Urban heat island research in Phoenix, Arizona: theoretical contributions and policy applications. *Bull. Am. Meteorol. Soc.* 93, 517–530. doi: 10.1175/bams-d-11-00011.1
- Churkina, G. (2008). Modeling the carbon cycle of urban systems. *Ecol. Model.* 216, 107–113. doi: 10.1016/j.ecolmodel.2008.03.006
- Churkina, G., Grote, R., Butler, T. M., and Lawrence, M. (2015). Natural selection? Picking the right trees for urban greening. *Environ. Sci. Policy* 47, 12–17. doi: 10.1016/j.envsci.2014.10.014
- de Kauwe, M. G., Kala, J., Lin, Y.-S., Pitman, A. J., Medlyn, B. E., Duursma, R. A., et al. (2015). A test of an optimal stomatal conductance scheme within the

manuscript. All authors contributed to the article and approved the submitted version.

FUNDING

This work was supported by the National Science Foundation grants DGE-1840990, ICER 1854706, and DGE 1735087 and NASA JPL award 80NSSC18K0959.

SUPPLEMENTARY MATERIAL

The Supplementary Material for this article can be found online at: <https://www.frontiersin.org/articles/10.3389/fevo.2021.695995/full#supplementary-material>

- CABLE land surface model. *Geosci. Model Dev.* 8, 431–452. doi: 10.5194/gmd-8-431-2015
- Decina, S. M., Hutyrá, L. R., Gately, C. K., Getson, J. M., Reinmann, A. B., Short Gianotti, A. G., et al. (2016). Soil respiration contributes substantially to urban carbon fluxes in the greater Boston area. *Environ. Pollut.* 212, 433–439. doi: 10.1016/j.envpol.2016.01.012
- Decina, S. M., Templer, P. H., and Hutyrá, L. R. (2018). Atmospheric inputs of nitrogen, carbon, and phosphorus across an urban area: unaccounted fluxes and canopy influences. *Earth's Future* 6, 134–148. doi: 10.1002/2017ef000653
- Decina, S. M., Templer, P. H., Hutyrá, L. R., Gately, C. K., and Rao, P. (2017). Variability, drivers, and effects of atmospheric nitrogen inputs across an urban area: emerging patterns among human activities, the atmosphere, and soils. *Sci. Total Environ.* 609, 1524–1534. doi: 10.1016/j.scitotenv.2017.07.166
- Dwyer, J. L., Roy, D. P., Sauer, B., Jenkerson, C. B., Zhang, H. K., and Lymburner, L. (2018). Analysis ready data: enabling analysis of the landsat archive. *Remote Sens.* 10:1363. doi: 10.3390/rs10091363
- Esperon-Rodriguez, M., Rymer, P. D., Power, S. A., Challis, A., Marchin, R. M., and Tjoelker, M. G. (2020). Functional adaptations and trait plasticity of urban trees along a climatic gradient. *Urban For. Urban Green.* 54:126771. doi: 10.1016/j.ufug.2020.12677
- EUMETSAT OSI SAF (2021a). *Geostationary Radiative Fluxes: GOES-E Downward Longwave Irradiance Product OSI-305-b*. Available online at: <https://osi-saf.eumetsat.int/products/osi-305-b> (accessed July 9, 2020).
- EUMETSAT OSI SAF (2021b). *Geostationary Radiative Fluxes: GOES-E Surface Solar Irradiance Product OSI-305-b*. Available online at: <https://osi-saf.eumetsat.int/products/osi-306-b> (accessed July 9, 2020).
- Fitzpatrick, M. C., and Dunn, R. R. (2019). Contemporary climatic analogs for 540 North American urban areas in the late 21st century. *Nat. Commun.* 10:614. doi: 10.1038/s41467-019-08540-3
- Gasparri, A., Guo, Y., Hashizume, M., Lavigne, E., Zanobetti, A., Schwartz, J., et al. (2015). Mortality risk attributable to high and low ambient temperature: a multicountry observational study. *Lancet* 386, 369–375. doi: 10.1016/S0140-6736(14)62114-0
- Gebauer, T., Horna, V., and Leuschner, C. (2008). Variability in radial sap flux density patterns and sapwood area among seven co-occurring temperate broad-leaved tree species. *Tree Physiol.* 28, 1821–1830. doi: 10.1093/treephys/28.12.1821
- Gorelick, N., Hancher, M., Dixon, M., Ilyushchenko, S., Thau, D., and Moore, R. (2017). Google earth engine: planetary-scale geospatial analysis for everyone. *Remote Sens. Environ.* 202, 18–27. doi: 10.1016/j.rse.2017.06.031
- Grimm, N. B., Faeth, S. H., Golubiewski, N. E., Redman, C. L., Wu, J., Bai, X., et al. (2008). Global change and the ecology of cities. *Science* 319, 756–760. doi: 10.1126/science.1150195
- Grimmond, C. S. B., Blackett, M., Best, M. J., Barlow, J., Baik, J.-J., Belcher, S. E., et al. (2010). The international urban energy balance models comparison project: first results from phase 1. *J. Appl. Meteorol. Climatol.* 45, 1268–1292. doi: 10.1175/2010JAMC2354.1

- Gu, Y., Hunt, E., Wardlow, B., Basara, J. B., Brown, J. F., and Verdin, J. P. (2008). Evaluation of MODIS NDVI and NDWI for vegetation drought monitoring using Oklahoma Mesonet soil moisture data. *Geophys. Res. Lett.* 35:L22401. doi: 10.1029/2008gl035772
- Habeeb, D., Vargo, J., and Stone, B. (2015). Rising heat wave trends in large US cities. *Nat. Hazards* 76, 1651–1665. doi: 10.1007/s11069-014-1563-z
- Hardiman, B. S., Wang, J. A., Hutrya, L. R., Gately, C. K., Getson, J. M., and Friedl, M. A. (2017). Accounting for urban biogenic fluxes in regional carbon budgets. *Sci. Total Environ.* 592, 366–372. doi: 10.1016/j.scitotenv.2017.03.028
- Hobbie, S. E., Finlay, J. C., Janke, B. D., Nidvvzgoriski, D. A., Millet, D. B. and Baker, L. A. (2017). Contrasting nitrogen and phosphorus budgets in urban watersheds and implications for managing urban water pollution. *Proc. Natl. Acad. Sci. U. S. A.* 114, 4177–4182. doi: 10.1073/pnas.1706049114
- Hoffman, J. S., Shandas, V., and Pendleton, N. (2020). The Effects of historical housing policies on resident exposure to intra-urban heat: a study of 108 us urban areas. *Climate* 8:12. doi: 10.3390/cli8010012
- Hollinger, D. (2021). *AmeriFlux US-Ho1 Howland Forest (Main Tower), Version 7-5, AmeriFlux AMP, (Dataset)*. Available online at: <https://doi.org/10.17190/AMF/1246061> (accessed August 3, 2020).
- Jones, T. S., Winbourne, J. B., and Hutrya, L. R. (2020). Ribbonized sap flow: an emerging technology for the integration of sap flow sensor components onto a single platform. *Ecosphere* 11:e03135. doi: 10.1002/ecs2.3135
- Li, D., Liao, W., Rigden, A. J., Liu, X., Wang, D., Malyshev, S., et al. (2019). Urban heat island: aerodynamics or imperviousness? *Sci. Adv.* 5:eau4299. doi: 10.1126/sciadv.aau4299
- Liu, X., Li, X.-X., Harshan, S., Roth, M., and Velasco, E. (2017). Evaluation of an urban canopy model in a tropical city: the role of tree evapotranspiration. *Environ. Res. Lett.* 12:094008. doi: 10.1088/1748-9326/aa7ee7
- Liu, Z., He, C., Zhou, Y., and Wu, J. (2014). How much of the world's land has been urbanized, really? A hierarchical framework for avoiding confusion. *Landsc. Ecol.* 29, 763–771. doi: 10.1007/s10980-014-0034-y
- Mahadevan, P., Wofsy, S. C., Matross, D. M., Xiao, X., Dunn, A. L., Lin, J. C., et al. (2008). A satellite-based biosphere parameterization for net ecosystem CO₂ exchange: vegetation photosynthesis and respiration model (VPRM). *Global Biogeochem. Cycles* 22:GB2005. doi: 10.1029/2006GB002735
- Maki, M., Ishihara, M., and Tamura, M. (2004). Estimation of leaf water status to monitor the risk of forest fires by using remotely sensed data. *Remote Sens. Environ.* 90, 441–450. doi: 10.1016/j.rse.2004.02.002
- Martilli, A., Krayenhoff, E. S., and Nazarian, N. (2020). Is the urban heat island intensity relevant for heat mitigation studies? *Urban Clim.* 31:100541. doi: 10.1016/j.uclim.2019.100541
- MassGIS. (2019). *MassGIS Data: Impervious Surface 2016*. Available online at: <https://www.mass.gov/info-details/massgis-data-2016-land-coverland-use> (accessed January 21, 2020).
- McCarthy, H. R., and Pataki, D. E. (2010). Drivers of variability in water use of native and non-native urban trees in the greater Los Angeles area. *Urban Ecosyst.* 13, 393–414. doi: 10.1007/s11252-010-0127-6
- McPherson, E. G., Nowak, D. J., and Rowntree, R. A. (1994). *Chicago's Urban Forest Ecosystem: Results of the Chicago Urban Forest Climate Project*. General Technical Report. NE-186. Radnor, PA: U.S. Department of Agriculture.
- Medlyn, B. E., Duursma, R. A., Eamus, D., Ellsworth, D. S., Prentice, I. C., Barton, C. V. M., et al. (2011). Reconciling the optimal and empirical approaches to modelling stomatal conductance. *Glob. Chang. Biol.* 17, 2134–2144. doi: 10.1111/j.1365-2486.2010.02375.x
- Melaas, E. K., Wang, J. A., Miller, D. L., and Friedl, M. A. (2016). Interactions between urban vegetation and surface urban heat islands: a case study in the Boston metropolitan region. *Environ. Res. Lett.* 11:054020. doi: 10.1088/1748-9326/11/5/054020
- Mell, I. C., Henneberry, J., Hehl-Lange, S., and Keskin, B. (2013). Promoting urban greening: valuing the development of green infrastructure investments in the urban core of Manchester, UK. *Urban For. Urban Green.* 12, 296–306. doi: 10.1016/j.ufug.2013.04.006
- Metzger, K. B., Ito, K., and Matte, T. D. (2010). Summer heat and mortality in New York city: how hot is too hot? *Environ. Health Perspect.* 118, 80–86. doi: 10.1289/ehp.0900906
- Monteith, J. L. (1965). Evaporation and environment. *Symp. Soc. Exp. Biol.* 19, 205–234.
- Munger, J. W. (2021). *AmeriFlux US-Ha1 Harvard Forest EMS Tower (HFR1), Version 16-5, AmeriFlux AMP, (Dataset)*. Available online at: <https://doi.org/10.17190/AMF/1246059> (accessed August 3, 2020).
- Munger, J. W., and Loeschner, H. W. (2004). *Guidelines for Making Eddy Covariance Flux Measurements*. Oakridge, TM: Ameriflux.
- Oke, T., Mills, G., Christen, A., and Voogt, J. (2017). *Urban Climates*. Cambridge: Cambridge University Press, doi: 10.1017/9781139016476
- Pataki, D. E., McCarthy, H. R., Litvak, E., and Pincetl, S. (2011). Transpiration of urban forests in the Los Angeles metropolitan area. *Ecol. Appl.* 21, 661–677. doi: 10.1890/09-1717.1
- Pincetl, S., Gillespie, T., Pataki, D. E., Saatchi, S., and Saphores, J.-D. (2013). Urban tree planting programs, function or fashion? Los Angeles and urban tree planting campaigns. *GeoJournal* 78, 475–493. doi: 10.1007/s10708-012-9446-x
- R Core Team. (2020). *R: A Language and Environment for Statistical Computing*. Vienna: R Foundation for Statistical Computing.
- Raciti, S. M., Hutrya, L. R., and Newell, J. D. (2014). Mapping carbon storage in urban trees with multi-source remote sensing data: relationships between biomass, land use, and demographics in Boston neighborhoods. *Sci. Total Environ.* 500, 72–83. doi: 10.1016/j.scitotenv.2014.08.070
- Rahman, M. A., Moser, A., Gold, A., Rötzer, T., and Pauleit, S. (2018). Vertical air temperature gradients under the shade of two contrasting urban tree species during different types of summer days. *Sci. Total Environ.* 633, 100–111. doi: 10.1016/j.scitotenv.2018.03.168
- Rahman, M. A., Moser, A., Rötzer, T., and Pauleit, S. (2017). Within canopy temperature differences and cooling ability of *Tilia cordata* trees grown in urban conditions. *Build. Environ.* 114, 118–128. doi: 10.1016/j.buildenv.2016.12.013
- Rao, P., Hutrya, L. R., Raciti, S. M., and Templer, P. H. (2014). Atmospheric nitrogen inputs and losses along an urbanization gradient from Boston to Harvard Forest, MA. *Biogeochemistry* 121, 229–245. doi: 10.1007/s10533-013-9861-1
- Reinmann, A. B., and Hutrya, L. R. (2017). Edge effects enhance carbon uptake and its vulnerability to climate change in temperate broadleaf forests. *Proc. Natl. Acad. Sci. U. S. A.* 114, 107–112. doi: 10.1073/pnas.1612369114
- Roman, L. A. (2014). How many trees are enough? Tree death and the urban canopy. *Scenario J. Scenario* 4, 1–8.
- Ruijven, B. J., Cian, E. D., and Wing, I. S. (2019). Amplification of future energy demand growth due to climate change. *Nat. Commun.* 10:2762. doi: 10.1038/s41467-019-10399-3
- Sargent, M., Barrera, Y., Nehrkorn, T., Hutrya, L. R., Gately, C. K., Jones, T., et al. (2018). Anthropogenic and biogenic CO₂ fluxes in the Boston urban region. *Proc. Natl. Acad. Sci. U. S. A.* 115, 7491–7496. doi: 10.1073/pnas.1803715115
- Seto, K. C., Güneralp, B., and Hutrya, L. R. (2012). Global forecasts of urban expansion to 2030 and direct impacts on biodiversity and carbon pools. *Proc. Natl. Acad. Sci. U. S. A.* 109, 16083–16088. doi: 10.1073/pnas.1211658109
- Smith, I. A. (2021). *Data for 'A Satellite-Based Model for Estimating Latent Heat Flux From Urban Vegetation.'* Available online at: <https://doi.org/10.7910/DVNI/TQLSIU>, Harvard Dataverse.
- Smith, I. A., Dearborn, V. K., and Hutrya, L. R. (2019). Live fast, die young: accelerated growth, mortality, and turnover in street trees. *PLoS One* 14:e0215846. doi: 10.1371/journal.pone.0215846
- Suyker, A. (2021). *AmeriFlux US-Ne1 Mead - Irrigated Continuous Maize Site, Version 11-5, AmeriFlux AMP, (Dataset)*. Available online at: <https://doi.org/10.17190/AMF/1246084> (accessed August 3, 2020).
- Taha, H. (1997). Urban climates and heat islands: albedo, evapotranspiration, and anthropogenic heat. *Energy. Build.* 25, 99–103. doi: 10.1016/S0378-7788(96)00999-1
- Tan, P. Y., Wang, J., and Sia, A. (2013). Perspectives on five decades of the urban greening of Singapore. *Cities* 32, 24–32. doi: 10.1016/j.cities.2013.02.001
- Tang, J., Bolstad, P. V., Desai, A. R., Martin, J. G., Cook, B. D., Davis, K. J., et al. (2008). Ecosystem respiration and its components in an old-growth forest in the Great Lakes region of the United States. *Agric. For. Meteorol.* 148, 171–185. doi: 10.1016/j.agrformet.2007.08.008
- Teskey, R., Wertin, T., Bauweraerts, I., Amey, M., Mcguire, M. A., and Steppe, K. (2014). Responses of tree species to heat waves and extreme heat events. *Plant Cell Environ.* 38, 1699–1712. doi: 10.1111/pce.12417

- Tiangco, M., Lagmay, A. M. F., and Argete, J. (2008). ASTER—based study of the night—time urban heat island effect in Metro Manila. *Int. J. Remote Sens.* 29, 2799–2818. doi: 10.1080/01431160701408360
- Trlica, A., Hutyra, L. R., Schaaf, C. L., Erb, A., and Wang, J. A. (2017). Albedo, land cover, and daytime surface temperature variation across an urbanized landscape. *Earth's Future* 5, 1084–1101. doi: 10.1002/2017EF000569
- United Nations Department of Economic and Social Affairs Population Division. (2018). *World Urbanization Prospects: The 2018 Revision*. New York, NY: United Nations.
- Urban, J., Ingwers, M., McGuire, M. A., and Teskey, R. O. (2017). Stomatal conductance increases with rising temperature. *Plant Signal. Behav.* 12:e1356534. doi: 10.1080/15592324.2017.1356534
- von Caemmerer, S., and Evans, J. R. (2015). Temperature responses of mesophyll conductance differ greatly between species. *Plant Cell Environ.* 38, 629–637. doi: 10.1111/pce.12449
- Wahid, A., Gelani, S., Ashraf, M., and Foolad, M. R. (2007). Heat tolerance in plants: an overview. *Environ. Exp. Bot.* 61, 199–223. doi: 10.1016/j.envexpbot.2007.05.011
- Wang, J. A., Hutyra, L. R., Li, D., and Friedl, M. A. (2017). Gradients of atmospheric temperature and humidity controlled by local urban land-use intensity in Boston. *J. Appl. Meteorol. Climatol.* 56, 817–831. doi: 10.1175/JAMC-D-16-0325.1
- Wang, Y., Zhang, Y., Ding, N., Qin, K., and Yang, X. (2020). Simulating the impact of urban surface evapotranspiration on the urban heat island effect using the modified RS-PM model: a case study of Xuzhou, China. *Remote Sens.* 12:578. doi: 10.3390/rs12030578
- Weber, F., Kowarik, I., and Säumel, I. (2014). Herbaceous plants as filters: immobilization of particulates along urban street corridors. *Environ. Pollut.* 186, 234–240. doi: 10.1016/j.envpol.2013.12.011
- Wellenius, G. A., Eliot, M. N., Bush, K. F., Holt, D., Lincoln, R. A., Smith, A. E., et al. (2017). Heat-related morbidity and mortality in New England: evidence for local policy. *Environ. Res.* 156, 845–853. doi: 10.1016/j.envres.2017.02.005
- Weston, D. J., and Bauerle, W. L. (2007). Inhibition and acclimation of C3 photosynthesis to moderate heat: a perspective from thermally contrasting genotypes of *Acer rubrum* (red maple). *Tree Physiol.* 27, 1083–1092. doi: 10.1093/treephys/27.8.1083
- Winbourne, J. B., Jones, T. S., Garvey, S. M., Harrison, J. L., Wang, L., Li, D., et al. (2020). Tree transpiration and urban temperatures: current understanding, implications, and future research directions. *BioScience* 70, 576–588. doi: 10.1093/biosci/biaa055
- Wong, N. H., Cheong, D. K. W., Yan, H., Soh, J., Ong, C. L., and Sia, A. (2003). The effects of rooftop garden on energy consumption of a commercial building in Singapore. *Energy Build.* 35, 353–364. doi: 10.1016/S0378-7788(02)00108-1
- Wullschleger, S. D., Hanson, P., and Todd, D. (2001). Transpiration from a multi-species deciduous forest as estimated by xylem sap flow techniques. *For. Ecol. Manag.* 143, 205–213. doi: 10.1016/s0378-1127(00)00518-1
- Zhang, L., and Dawes, W. R. (1995). *Influence of Atmospheric Stability Upon Evapotranspiration Estimates—Tests Using HAPEX-MOBILHY Data and the WAVES Model, Technical Memorandum/CSIRO, Institute of Natural Resources and Environment, Division of Water Resources. 95.1*. Melbourne, VIC: CSIRO.
- Zhang, Y., Li, L., Qin, K., Wang, Y., Chen, L., and Yang, X. (2018). Remote sensing estimation of urban surface evapotranspiration based on a modified Penman–Monteith model. *J. Appl. Remote Sens.* 12:046006. doi: 10.1117/1.JRS.12.046006
- Zhang, Y. Q., Chiew, F. H. S., Zhang, L., Leuning, R., and Cleugh, H. A. (2008). Estimating catchment evaporation and runoff using MODIS leaf area index and the Penman–Monteith equation. *Water Resour. Res.* 44:W10420. doi: 10.1029/2007WR006563
- Zhou, W., Fisher, B., and Pickett, S. T. (2019). Cities are hungry for actionable ecological knowledge. *Front. Ecol. Environ.* 17:135–135. doi: 10.1002/fee.2021
- Zipper, S. C., Schatz, J., Kucharik, C. J., and Loheide, S. P. (2017). Urban heat island-induced increases in evapotranspirative demand. *Geophys. Res. Lett.* 44, 873–881. doi: 10.1002/2016GL072190
- Ziter, C. D., Pedersen, E. J., Kucharik, C. J., and Turner, M. G. (2019). Scale-dependent interactions between tree canopy cover and impervious surfaces reduce daytime urban heat during summer. *Proc. Natl. Acad. Sci. U. S. A.* 116, 7575–7580. doi: 10.1073/pnas.1817561116

Conflict of Interest: The authors declare that the research was conducted in the absence of any commercial or financial relationships that could be construed as a potential conflict of interest.

Publisher's Note: All claims expressed in this article are solely those of the authors and do not necessarily represent those of their affiliated organizations, or those of the publisher, the editors and the reviewers. Any product that may be evaluated in this article, or claim that may be made by its manufacturer, is not guaranteed or endorsed by the publisher.

Copyright © 2021 Smith, Winbourne, Tieskens, Jones, Bromley, Li and Hutyra. This is an open-access article distributed under the terms of the Creative Commons Attribution License (CC BY). The use, distribution or reproduction in other forums is permitted, provided the original author(s) and the copyright owner(s) are credited and that the original publication in this journal is cited, in accordance with accepted academic practice. No use, distribution or reproduction is permitted which does not comply with these terms.